

Novel three-dimensional optimal path planning method for vehicles with constrained pitch and yaw

B. Wehbe, S. Bazzi and E. Shammas*

Department of Mechanical Engineering, American University of Beirut, Beirut, Lebanon. E-mails: biw00@aub.edu.lb, smb20@aub.edu.lb

(Accepted October 8, 2016. First published online: November 2, 2016)

SUMMARY

This paper presents a novel method for generating three-dimensional optimal trajectories for a vehicle or body that moves forward at a constant speed and steers in both horizontal and vertical directions. The vehicle's dynamics limit the body-frame pitch and yaw rates; additionally, the climb and decent angles of the vehicle are also bounded. Given the above constraints, the path planning problem is solved geometrically by building upon the two-dimensional Dubins curves and then Pontryagin's Maximum Principle is used to validate that the proposed solution lies within the family of candidate time-optimal trajectories. Finally, given the severe boundedness constraints on the vertical motion of the system, the robustness of the proposed path planning method is validated by naturally extending it to remain applicable to high-altitude final configurations.

KEYWORDS: Three-dimensional path planning; Trajectory generation; Optimal paths; Dubins paths; Non-holonomic motion planning; Underwater autonomous vehicles.

1. Introduction

Guiding a robotic platform between any two given configurations along a time-optimal trajectory is a problem of great interest in the field of robotics and locomotion, especially when energy-efficient movements are desired. This problem gets more complicated when motion constraints are added to the system. For example, mechanical constraints on the steering angle impose a maximum curvature (or minimum turning radius) constraint on the path of a car-like robot, unlike a differentially driven robot, which can rotate in place. Unmanned aerial and underwater vehicles, with a single propulsive thruster and steering wings or fins, exhibit similar “steering” constraints in both pitch and yaw.

Markov¹⁴ first posed the problem of finding the shortest planar path connecting two points with specified orientation vectors for a vehicle moving forward with a constant speed and subjected to a constraint on maximum curvature. The constant speed assumption reposed the problem as finding the time-optimal trajectory between two arbitrary vectors in the plane. By employing a geometric approach, Dubins⁵ attempted to solve this problem by using motion primitives composed of only straight lines and circles. The shortest “R-geodesics”, so called by Dubins, were necessarily a concatenation of at most three segments, each of which is a straight line (S) or an arc of a circle (C) of minimum turning radius (maximum curvature). These include (S), (C), (SC), (CS), (CSC), (CCC), some of which are depicted in Fig. 1.

Building upon the results of Dubins, Reeds and Shepp²⁰ extended the set of optimal paths by considering a vehicle that could move both forward and backward. They showed that the optimal trajectories for such a vehicle are composed of concatenations of straight lines and circles of five pieces at most, and classified them into 48 different “words” or families. Boissonnat et al.³ were able to reproduce the results of Dubins and Reeds and Shepp by taking recourse to optimal control theory and specifically Pontryagin's Maximum Principle (PMP).¹⁹ In a worked out example for the Reeds-Shepp car, Sussmann and Tang²² combined the technique of the maximum principle with geometric methods based on Lie algebra to improve upon the result of Reeds and Shepp in ref. [20], reducing

* Corresponding author. E-mail: es34@aub.edu.lb

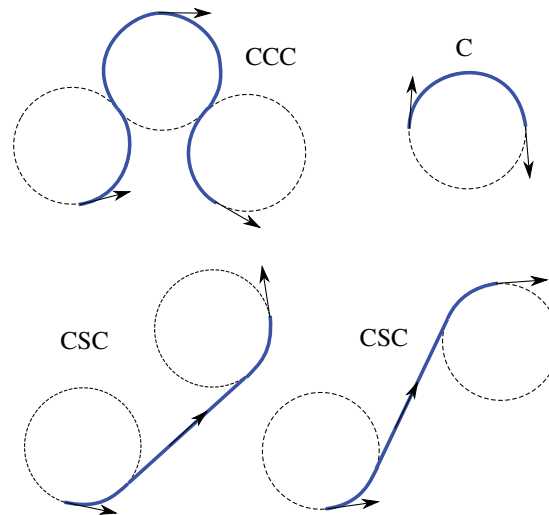


Fig. 1. Examples of the Dubins paths.

their 48 families of curves to 46. A generalized set of optimal trajectories for steered cars in the plane was formulated by Furtuna and Balkcom⁷ by using the PMP once again. Balluchi et al.² implemented path tracking control for a Dubins car by using a discontinuous control scheme based on the theory of sliding modes control. Jiang et al.¹⁰ presented an optimal motion planning strategy that generates minimum-time, first-derivative-smooth paths for a mobile robot. Finally, Xidias and Aspragathos²⁶ developed a geometrical approach for generating simultaneously optimal smooth paths for a set of non-holonomic robots.

Although time-optimal trajectories for two-dimensional (2D) platforms have been well determined, finding 3D optimal paths is still an active area of research. Working on underwater gliders, Mahmoudian et al.¹³ used planar Dubins curves as a tool for the path planning by projecting the start and end configuration on a horizontal plane thus neglecting any cost for the vertical component of motion. McGee and Hedrick¹⁵ also considered the same 2D case for an aerial vehicle. Chitsaz and LaValle⁴ studied the time-optimal paths for a *Dubins airplane*, which consists of a Dubins car model with an additional altitude coordinate. The limitation of this model lies in the fact that it neglects both pitch and roll rotations. PMP was also used by Chitsaz and LaValle to prove that their time-optimal trajectories are a concatenation of circles, straight lines, and pieces of planar elastica. The planar elastica segments arise after imposing an energy-based constraint. Gal and Doytsher⁸ developed a local trajectory planner for an unmanned aerial vehicle, taking into account kinematic and dynamic constraints. However, they used an airplane model similar to that of Chitsaz and LaValle. Moreover, the planner generated the most “visible” trajectories, rather than the optimal ones.

Sampling-based motion planning algorithms opened the horizon to new approaches such as RRT (feasible path planning), RRT* (optimal path planning given a steering function),¹¹ and modern approaches that utilize random shooting/forward propagation for non-linear problems.^{12, 17, 18} It is worth noting, that such approaches are search-based even though some of them do produce optimal paths. However, the methods presented in this paper produced explicit analytical solution paths for the motion planning problem.

Neto and Campos¹⁶ proposed an iterative algorithm based on the model of a fifth-order spatial Bézier curve to generate sub-optimal paths that satisfy maximum curvature, torsion, and climbing angle constraints. Hota and Ghose⁹ proposed a geometric method that generates paths composed of straight lines and circles; however, this method does not always produce optimal paths and in some cases generates paths that are not flyable by a real vehicle with a constraint on maximum pitch angle. In the case when a high pitch angle is required, Hota and Ghose also presented a numerical method based on a multiple shooting algorithm, which came at the cost of complexity and high computational power.

The field of biomedical engineering also took benefit of Dubins paths, where Alterovitz et al.¹ and Duindam et al.⁶ modeled the motion of a surgical needle through the body as kinematically equivalent to an airplane with fixed speed and pitch rate, zero yaw, and controllable roll rate. Webster et al.²³ studied the design and experimental validation of a non-holonomic model for steering flexible needles with beveled tips; their model generalized the unicycle model to a six degrees of freedom model by using Lie group theory. Finally, by applying optimal control theory on manifolds, Sussmann²¹ studied 3D curves with maximum curvature constraint and proved that minimizers in three-dimensions are not only a three-piece concatenation of straight lines and circles but also a *helicoidal arc* with a non-zero torsion. In his paper, Sussmann only applied a curvature constraint to general 3D curves while not addressing any pitch or flight angle constraints, and hence the resulting paths may not be dynamically feasible.

In an earlier work, Wehbe et al.^{24,25} proposed a geometric method for generating 3D paths for a vehicle with constrained curvature in both the pitch and yaw rotation directions. However, the optimality of the proposed method was not assessed.

In this paper, the motivation is to plan feasible paths, which respect the motion constraints of a real robotic platform, specifically the limited action of the control actuators. Such constraints can be sub-divided into (i) a yaw or heading curvature constraint that is similar to the case of the planar Dubins car, (ii) a pitch curvature constraint that is represented as a minimum radius in a vertical sense, and (iii) a maximum allowable pitch angle constraint. The main contribution of this paper is the formulation of a novel path planning method that generates optimal yet feasible 3D trajectories in an obstacle free environment, from a start to a goal configuration, taking into account the constraints mentioned above. The proposed approach is based on an intuitive, yet robust integration of two 2D optimal paths to generate the required 3D path. Moreover, we take recourse to the PMP as a necessary condition to verify that the generated paths are a subset of the set of possible optimal trajectories. To test the robustness of the proposed approach, its applicability to the so called “high-altitude” configurations is investigated.

This paper is organized into four main sections. In Section 2, the kinematic model that captures the typical motion of 3D robotic platforms is presented, and the motion planning problem is defined. In Section 3, the proposed geometric approach for finding 3D optimal paths is described, and the control law for tracing these paths is derived. In Section 4, PMP is used to derive a set of candidate time-optimal paths for 3D maneuvering vehicles and we show that the paths emerging from the geometric approach lie within this set. Section 5 investigates the robustness of the proposed method with respect to high-altitude configurations. Some simulation results are presented in Section 6. Finally, Sections 7 and 8 conclude the paper and raise some points worthy of discussion.

2. Problem Formulation

In this section, a five degrees of freedom kinematic model describing the motion of a robotic platform maneuvering in 3D space is presented. Moreover, the motion planning problem of such a platform, under curvature constraints on both pitch and heading, is stated explicitly.

2.1. The model

The vehicle is modeled as a rigid body that maneuvers in 3D space. It is capable of propelling itself forward as well as steering in both the horizontal and vertical directions. To study the kinematics of the vehicle’s motion, two Cartesian coordinate frames are utilized; an inertial or fixed frame $\{\mathbf{F}_i : (x, y, z)\}$ and a body or moving frame $\{\mathbf{F}_b : (x_b, y_b, z_b)\}$, as shown in Fig. 2. The motion of the body can be described using five generalized coordinates; the position coordinates $(x, y, z) \in \mathbb{R}^3$ and the orientation coordinates (θ, ψ) . Assuming the roll is passively stable, the orientation coordinates are specified as the pitch angle $\theta \in]-\frac{\pi}{2}, \frac{\pi}{2}[$, and the heading angle $\psi \in]-\pi, \pi]$. The body frame \mathbf{F}_b is considered to be attached to some point on the body (usually the center of mass) and is used to capture the body velocities, namely, the linear velocities (u, v, w) and angular velocities (p, h) . Assuming the vehicle moves forward with a constant unit speed, and no lateral and vertical body velocity components, we set $u = 1$, $v = 0$, and $w = 0$. The turning or angular velocities are specified as the pitch angular velocity p , and the heading angular velocity h . Accordingly, the full kinematic model can be represented by the following equations:

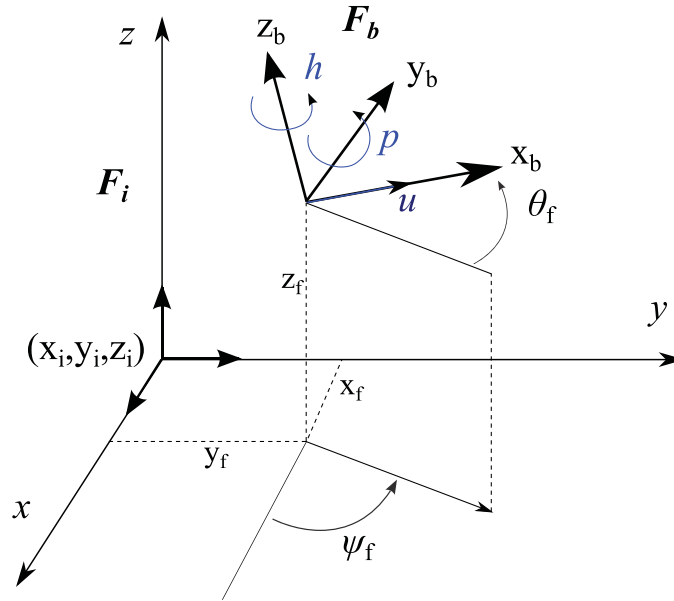


Fig. 2. Inertial and body coordinate frames.

$$\begin{aligned}
 \dot{x}(t) &= \cos \psi(t) \cos \theta(t), \\
 \dot{y}(t) &= \sin \psi(t) \cos \theta(t), \\
 \dot{z}(t) &= \sin \theta(t), \\
 \dot{\theta}(t) &= u_p(t), \\
 \dot{\psi}(t) &= u_h(t),
 \end{aligned}
 \tag{1}$$

where direct control is assumed over the pitch and heading rotational velocities, $\dot{\theta}(t)$ and $\dot{\psi}(t)$, respectively, through the control actions $u_p(t)$ and $u_h(t)$. The vehicle’s motion is assumed to be constrained by a minimum turning radius in both pitch and heading rotation. Without loss of generality, we will assume *unit* minimum turning radii. Accordingly, the last two equations in the above kinematic model can be expressed as

$$\begin{aligned}
 \dot{\theta}(t) &= u_p, \quad |u_p| \leq 1 \\
 \dot{\psi}(t) &= u_h, \quad |u_h| \leq 1.
 \end{aligned}
 \tag{2}$$

The 3D motion planning problem is formulated below.

2.2. Motion planning problem

Assuming an obstacle-free environment, and given a start and a final configuration in 3D space, $q_i = (0, 0, 0, 0, 0)$ and $q_f = (x_f, y_f, z_f, \theta_f, \psi_f)$, respectively, find the continuous curve of minimal length that joins the positions and is tangent to the orientations at these configurations such that the maximum bounds on pitch and heading curvatures are respected at all times, that is, $|\dot{\theta}| \leq 1$ and $|\dot{\psi}| \leq 1$. Additionally, the absolute constraint on the climb angle must also be satisfied, that is, $|\theta| \leq \theta_{\max} < \frac{\pi}{2}$.

Specifically, the inputs to the algorithm devised in this paper are the initial and final postures, q_i and q_f , respectively, and the output is a 3D trajectory traced by the kinematic model in Eq. (1), along with two control functions $u_p(t)$ and $u_h(t)$, given in Eq. (2), and the total time, $T \in]0, \infty[$, required to trace the path.

3. Geometric Method

In this section, a novel geometric method for generating optimal 3D trajectories, for any given initial and final configurations of the vehicle, is developed. The solution curve types that emerge are traced using a derived control law, toward the end of this section.

3.1. The approach

The proposed approach for optimal path planning in 3D is based upon integrating two Dubins paths; a horizontal one and vertical one. This is done by first dividing the path planning problem into two sub-problems; a horizontal one, or sub-problem 1, and a vertical one, sub-problem 2. The resulting sub-problems are shown below, where the superscripts “h” and “v” denote horizontal and vertical, respectively.

$$\begin{aligned}
 \text{Sub-problem 1: } & \begin{cases} q_i^h = (0, 0, 0) \\ q_f^h = (x_f, y_f, \psi_f) \end{cases} \\
 \text{Sub-problem 2: } & \begin{cases} q_i^v = (0, 0, 0) \\ q_f^v = (\bar{x}_f, z_f, \theta_f) \end{cases} . \tag{3}
 \end{aligned}$$

Note that all initial and final configurations specified in the sub-problems above are acquired from the motion planning problem in 2.2, except for \bar{x}_f , which denotes the arc length of the solution trajectory of sub-problem 1, as will be explained below. Accordingly, sub-problem 1 must be solved before sub-problem 2.

The method with which 3D time-optimal paths are generated using these two sub-problems is as follows. First, the original five-dimensional motion planning problem defined in 2.2 is projected onto the horizontal plane, rendering the problem a typical Dubins one. This gives rise to sub-problem 1, the solution of which is referred to as a *horizontal Dubins path* and is denoted by Γ_h . Next, the horizontal Dubins path, Γ_h , is extruded to form a “Dubins surface” normal to the $x - y$ plane. If the Dubins surface contains any cylindrical regions, in other words if the horizontal Dubins path comprises circular arcs, then these should be straightened out by unfolding them in order to form a planar surface of length equal to the total arc length of Γ_h . Thus, the length of the resulting planar surface is $\bar{x}_f = ||\Gamma_h||$. Assuming a generalized Dubins solution of the form (CSC), the lengths of the first and second circular arc segments are denoted by a_h and b_h , respectively, whereas c_h denotes the length of the straight line segment.

Following that, the height of the resulting Dubins surface is taken to be equal to z_f . By appending θ_f to the dimensions of this new Dubins surface, namely $||\Gamma_h||$ and z_f , the Dubins surface now defines the vertical portion of the original planning problem, which is nothing but sub-problem 2. In the plane of the Dubins surface, sub-problem 2 is a typical Dubins problem; one of joining two points with arbitrary orientations in a plane, and thus the solution will be a typical Dubins path. We refer to the solution of this sub-problem as a *vertical Dubins path*, denoted by Γ_v . Again, assuming a generalized Dubins solution of the form (CSC), the circular arc segments are denoted by a_v and b_v , respectively, whereas c_v denotes the length of the straight line segment.

Finally, to reconstruct the 3D path from Γ_h and Γ_v , the Dubins surface is folded back along the edges of the horizontal arcs a_h and b_h , to retain its original shape. Figure 3 provides a graphical depiction of the proposed geometric method described above.

It is important to note that the for a 3D solution to exist, the length of the horizontal path must be greater than zero. Dubins⁵ has proved that for non-trivial final configuration, a minimum length path is guaranteed to exist such that it has a non-zero length. However, since in this paper, the q_f^h is a projection of q_f on the horizontal plane, there is a possibility for $q_f^h \equiv q_i^h$. In such a case, the length of the horizontal path is zero, that is, $\bar{x}_f = ||\Gamma_h|| = 0$. To mitigate this problem, one needs to lengthen the horizontal sub-problem solution without violating the minimum steering radius and while ensuring that the boundary conditions are satisfied. In this paper, the horizontal path is lengthened whenever needed by adding a complete circle that is tangent anywhere to the horizontal path. In fact, even for the trivial case, ($q_f^h \equiv q_i^h$), one can still add a circle that is tangent to either q_i^h or q_f^h .

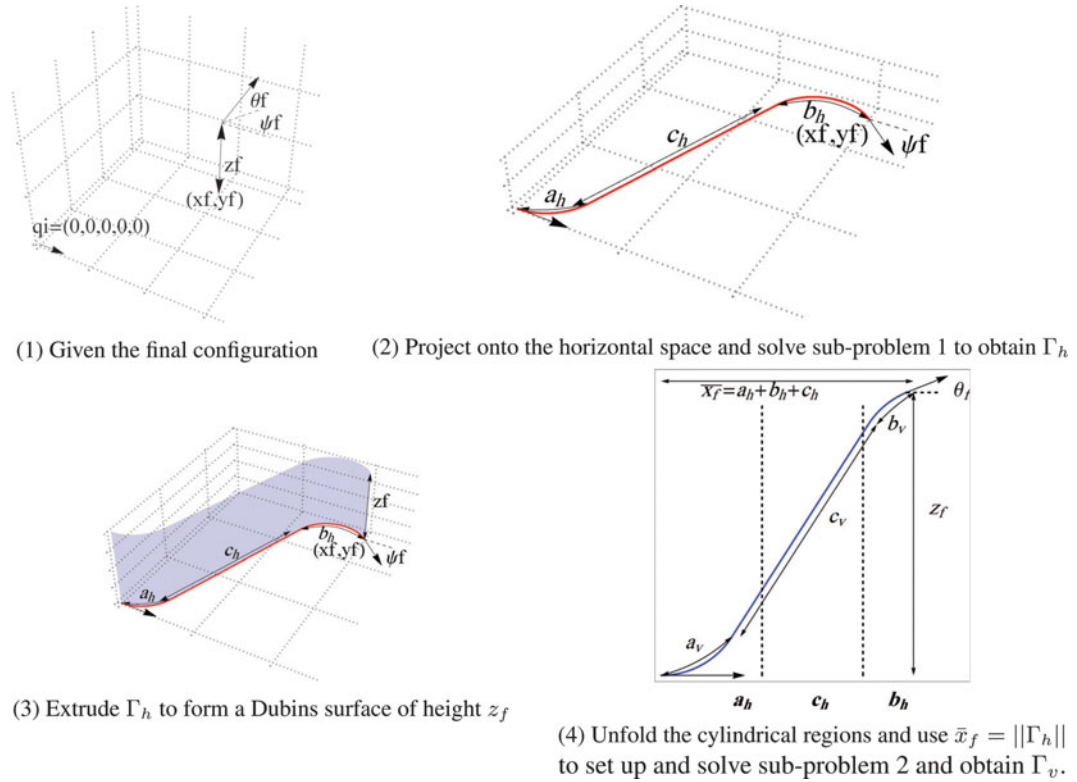


Fig. 3. The proposed geometric method. The 3D path is obtained by folding back along the dotted lines in the final step.

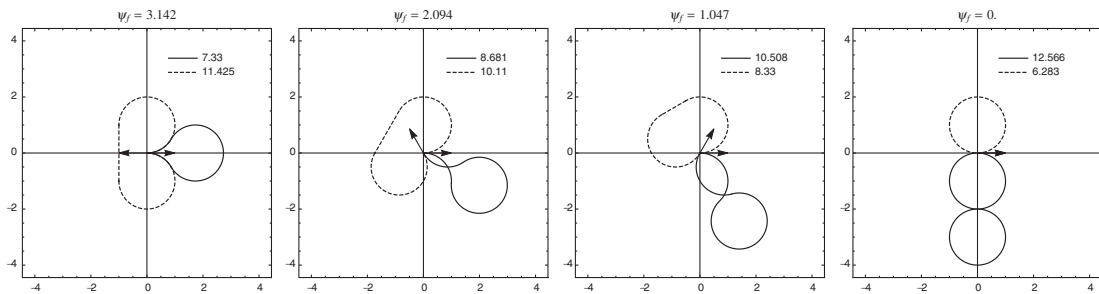


Fig. 4. Variation of the horizontal Dubins paths as ψ_f approaches 0.

To validate that adding a complete circle to the horizontal path is always valid and feasible, consider the following boundary conditions, $q_i^h = (0, 0, 0)$ and $q_f^h = (0, 0, \psi_f)$. The final steering angle ψ_f is varied from π to 0 as depicted in Fig. 4. In the same figure, both the CSC and CCC are also depicted. Note that as ψ_f tends to 0, the CSC curve tends to a single circle with a minimum turning radius whereas the CCC curve tends to two circles with a minimum turning radius. Both additions of circles lengthen the length of the horizontal curve, thus ensuring that $\bar{x}_f = \|\Gamma_h\| > 0$.

3.2. Solution curve types

As mentioned earlier, the control inputs of the system are the heading and pitch rotational velocities, u_h and u_p , respectively. Assuming a minimum turning radius $R = 1$ when the input is saturated in both the heading and pitch directions, the control region is the convex set $U = [-1, 1] \times [-1, 1]$, such that $(u_h, u_p) \in U$. In the above proposed construction, four types of extremal curves emerge as candidates for 3D time-optimal paths:

- (1) *Curve C*—An arc of a circle: This curve is obtained when the horizontal Dubins path segment is a straight line and the vertical segment is an arc, i.e., when $u_h = 0$ and u_p is saturated.

Table I. Possible 3D paths with their corresponding conditions.

Five-piece 3D path	Condition
H_2, H_1, S, H_1, H_2	$a_h > a_v$ and $b_h > b_v$
H_2, C, S, H_1, H_2	$a_h < a_v$ and $b_h > b_v$
H_2, H_1, S, C, H_2	$a_h > a_v$ and $b_h < b_v$
H_2, C, S, C, H_2	$a_h < a_v$ and $b_h < b_v$
H_2, S, H_2	$a_h = a_v$ and $b_h = b_v$

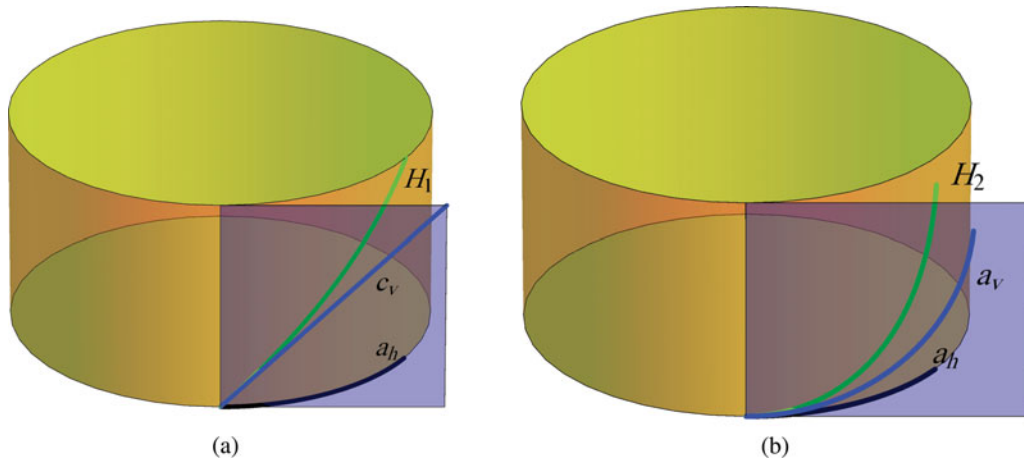


Fig. 5. Typical shapes of curves (a) H_1 and (b) H_2 .

- (2) *Curve S—A straight line:* This curve is obtained when both the vertical and horizontal Dubins curves are in the form of a straight line. In other words, it is obtained when both $u_h = 0$ and $u_p = 0$.
- (3) *Curve H_1 —A helix with a constant torsion:* This curve is obtained when $u_p = 0$ and u_h is saturated while the pitch angle θ is non-zero (when the horizontal Dubins path segment is an arc and the vertical one is a straight line). If $\theta = 0$, then the path becomes a circle in a plane parallel to the $x - y$ plane.
- (4) *Curve H_2 —A helix-like curve with non-constant torsion:* This curve is obtained when both control inputs are saturated, i.e., $u_p, u_h = \pm 1$ (when the segments of both the horizontal and vertical Dubins paths are arcs). Figure 5 illustrates curves H_1 and H_2 , to further clarify their shapes.

Table I lists all the possible resulting configurations of the 3D path, where the configuration is determined by comparing the lengths of the circular arcs of the horizontal and vertical Dubins paths, (a_h, b_h) and (a_v, b_v) , respectively. One can conclude from Table I that all possible resulting 3D paths consist of *five* sub-paths having the following order:

$$H_2 \rightarrow \begin{pmatrix} H_1 \\ \text{or} \\ C \end{pmatrix} \rightarrow S \rightarrow \begin{pmatrix} C \\ \text{or} \\ H_1 \end{pmatrix} \rightarrow H_2.$$

In other words, for a (CSC) solution for both horizontal and vertical Dubins curves, all resulting 3D paths will start and end with an H_2 -type curve, have an S -type middle segment, and the second and fourth portions of the curve will either be a C -type or H_1 -type. Note that in the special case that $a_h = a_v$ and $b_h = b_v$, then the generic 3D path reduces to *three* sub-paths instead of five. Also, the (CCC) solution of the horizontal Dubins curve will be discussed in Section 5.

3.3. Control law

In this section, some of the possible 3D paths that may emerge using the proposed geometric method are presented. Moreover, the motion of the vehicle (using the kinematic model (1)) is simulated along these paths, and the control inputs required to trace each path are provided.

Assuming a 3D path of the form (H_2, H_1, S, H_1, H_2) , the following control laws are used to trace the full 3D path:

$$u_h = \begin{cases} \pm 1 & \text{if } t \in [0, t_{h1}] \\ 0 & \text{if } t \in [t_{h1}, t_{h2}] , \\ \pm 1 & \text{if } t \in [t_{h2}, t_f] \end{cases} \tag{4}$$

$$u_p = \begin{cases} \pm 1 & \text{if } t \in [0, a_v] \\ 0 & \text{if } t \in [a_v, a_v + c_v] , \\ \pm 1 & \text{if } t \in [a_v + c_v, t_f] \end{cases} \tag{5}$$

where $t_{h1} = \|H_2\| + \|H_1\|$, $t_{h2} = t_{h1} + \|S\|$, and $t_f = a_v + b_v + c_v$.

Figure 6(a) depicts an example of such a curve, followed by its scheduled control inputs. In this case, the length of the first arc in the horizontal Dubins curve Γ_h is greater than its corresponding arc in the vertical curve Γ_v , and therefore the resulting curve type is H_1 , which is a result of the saturation of the heading control ($u_h = 1$) and setting the pitch control to zero ($u_p = 0$).

On the other hand, assuming a 3D path of the form (H_2, C, S, H_1, H_2) , i.e., when $a_v > a_h$ and $b_v < b_h$, the above control laws can be used such that $t_{h1} = \|H_2\|$ and $t_{h2} = t_{h1} + \|C\| + \|S\|$. An example of such a case is depicted in Fig. 6(b).

3.4. Path planning algorithm

The full path planning method proposed herein can be summarized in the following algorithm:

Algorithm 1 Path planning algorithm

- 1: Assuming an initial state $(0, 0, 0, 0, 0)$ and given a five-state final configuration $(x_f, y_f, z_f, \theta_f, \psi_f)$.
 - 2: Use (x_f, y_f, ψ_f) to set up and solve sub-problem 1 of the motion planning problem, thereby obtaining the horizontal Dubins curve, Γ_h .
 - 3: From Γ_h , obtain a_h, b_h , and c_h . Use these to calculate $\bar{x}_f = \|\Gamma_h\| = \|a_h\| + \|b_h\| + \|c_h\|$.
 - 4: Use $(\bar{x}_f, z_f, \theta_f)$ to set up and solve sub-problem 2 of the motion planning problem, thereby obtaining the vertical Dubins curve, Γ_v .
 - 4: From Γ_v , obtain a_v, b_v , and c_v .
 - 5: Calculate the length of each sub-path of the fully constructed 3D path to infer t_{h1}, t_{h2} , and t_f .
 - 6: Generate the control law for the vehicle's kinematic model using Eqs. (4) and (5).
-

4. Pontryagin's Maximum Principle

We use PMP to validate that the solution curve types, obtained using the geometric method proposed herein, lie within the family of candidate time-optimal trajectories. Using the PMP, the problem of finding the minimum-time trajectories for the vehicle reduces to finding a piecewise continuous control function $u^*(t)$ that drives the generalized coordinates of the system $q = (x, y, z, \theta, \psi)$ from an initial to a goal position, while in the same time minimizing a cost functional $J(u)$.

Accordingly, the control problem is stated as follows. Given the first-order differential state system $\dot{q}(t) = f(q(t), u(t))$ of a 3D maneuvering vehicle in a Cartesian coordinate frame stated in Eq. (1), where $u_p(t) \in [-1, 1]$ and $u_h(t) \in [-1, 1]$ are considered to be piecewise continuous controls corresponding respectively to the vehicle's pitch and heading rotational velocities, find the optimal controls $u^*(t) = (u_p^*(t), u_h^*(t))$ among all admissible controls, that transfer the system from an initial condition q_i to a final condition q_f , while minimizing the cost functional

$$J(u) = \int_0^T 1 dt \tag{6}$$

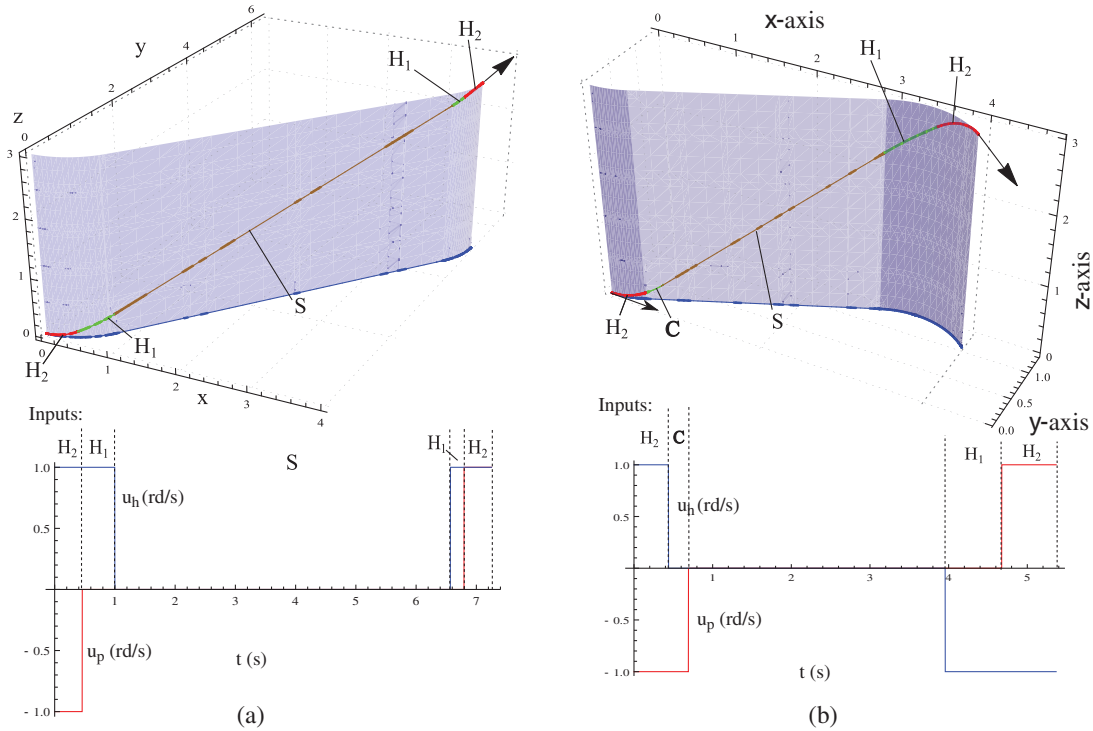


Fig. 6. (a) 3D path of type (H_2, H_1, S, H_1, H_2) , where $(x_f = 4, y_f = 5, z_f = 3, \psi_f = 90^\circ, \theta_f = 0^\circ)$ with the control input, (b) 3D path of type (H_2, C, S, H_1, H_2) , where $(x_f = 4, y_f = 1, z_f = 3, \psi_f = -45^\circ, \theta_f = 0^\circ)$ with the control input.

where $J(u)$ represents the travel time from q_i to q_f . The Hamiltonian of the system is given by

$$\begin{aligned}
 H(\lambda, q, u) &= \langle \lambda, \dot{q} \rangle + J(u) \\
 &= \lambda_1 \cos \psi \cos \theta + \lambda_2 \sin \psi \cos \theta + \lambda_3 \sin \theta + \lambda_4 u_p + \lambda_5 u_h + 1.
 \end{aligned}
 \tag{7}$$

The maximum principle states that for every optimal path associated with an optimal control u^* there exists a non-zero, continuous, and piecewise C^1 adjoint vector $\lambda = (\lambda_1, \lambda_2, \lambda_3, \lambda_4, \lambda_5)$ such that the following holds:

- (1) The adjoint vector is a solution of the Pontryagin's adjoint differential system

$$\frac{d\lambda_i}{dt} = -\frac{\partial H}{\partial q_i}.
 \tag{8}$$

- (2) The control $u^*(t)$ must be chosen to maximize the Hamiltonian at every instant t , that is,

$$H(\lambda(t), q(t), u^*(t)) = \max_u H(\lambda(t), q(t), u(t)).
 \tag{9}$$

- (3) The Hamiltonian of the system is a constant positive real number

$$H(\lambda(t), q(t), u^*(t)) = K.
 \tag{10}$$

Using Eq. (8), the adjoint system of equations reduces to

$$\begin{aligned}\dot{\lambda}_1(t) &= -\frac{\partial H}{\partial x} = 0, \\ \dot{\lambda}_2(t) &= -\frac{\partial H}{\partial y} = 0, \\ \dot{\lambda}_3(t) &= -\frac{\partial H}{\partial z} = 0, \\ \dot{\lambda}_4(t) &= -\frac{\partial H}{\partial \theta} = \lambda_1 \cos \psi \sin \theta + \lambda_2 \sin \psi \sin \theta - \lambda_3 \cos \theta + \lambda_5 u_h, \\ \dot{\lambda}_5(t) &= -\frac{\partial H}{\partial \psi} = \lambda_1 \sin \psi \cos \theta - \lambda_2 \cos \psi \cos \theta = \lambda_1 \dot{y} - \lambda_2 \dot{x}.\end{aligned}\quad (11)$$

By direct integration of Eq. (11), one first solves for λ_1 , λ_2 , λ_3 , and λ_5 yielding,

$$\begin{aligned}\lambda_1(t) &= c_1, \\ \lambda_2(t) &= c_2, \\ \lambda_3(t) &= c_3, \\ \lambda_5(t) &= c_1 y - c_2 x + c_5,\end{aligned}\quad (12)$$

where c_1 , c_2 , c_3 , and c_5 are all constants. By substituting the adjoint components of Eq. (12) into the Hamiltonian equation in (7), the resulting Hamiltonian is

$$H = c_1 \cos \psi \cos \theta + c_2 \sin \psi \cos \theta + c_3 \sin \theta + \lambda_4 u_p + \lambda_5 u_h + 1. \quad (13)$$

Next, the control inputs are chosen such that they maximize the Hamiltonian for every instant t as specified by the second condition of the maximum principle. Thus, a time-optimal trajectory associated to the adjoint vector λ , could be determined by a control law based on Eq. (9) and stated as follows:

$$\begin{cases} u_p = \text{sign}(\lambda_4) & \text{if } \lambda_4 \neq 0 \\ u_p \in [-1, 1] & \text{if } \lambda_4 = 0 \end{cases}, \quad (14)$$

$$\begin{cases} u_h = \text{sign}(\lambda_5) & \text{if } \lambda_5 \neq 0 \\ u_h \in [-1, 1] & \text{if } \lambda_5 = 0 \end{cases}. \quad (15)$$

Using the preceding control laws, the family of extremal paths can be categorized into four types of trajectories, described below.

Type 1: ($\lambda_4 = 0$ and $\lambda_5 = 0$) In this case, the path is a straight line segment with a direction determined by some fixed values of θ and ψ .

Proof. If $\lambda_5 = 0$, then the path follows a straight line in the (x, y, ψ) -space of equation $c_1 y - c_2 x + c_5 = 0$, with a direction $\psi = \arctan(\frac{c_2}{c_1})$. Moreover, if $\lambda_4 = 0$, that is, $\lambda_4 = 0$, then $c_1 \cos \psi \sin \theta + c_2 \sin \psi \sin \theta - c_3 \cos \theta = 0$. Again, given the boundedness of the pitch angle, namely, the fact that $\theta \neq \pm \frac{\pi}{2}$, then $(c_1 \cos \psi + c_2 \sin \psi) \tan \theta = c_3$. In other words, θ is a constant. \square

Type 2: ($\lambda_4 = 0$ and $\lambda_5 \neq 0$) In this case, the Hamiltonian $H(\lambda, q, u)$ is independent of λ_4 and the projection of the path onto (x, y, ψ) -space is a trajectory that must satisfy the PMP. Thus, the projection of the 3D path onto (x, y) -plane is a *Dubins* time-extremal path.

Proof. If $\lambda_4 = 0$, then the pitch control u_p can take any value in $[-1, 1]$. In this case, the 3D path is projected onto the (x, y, ψ) -space, eliminating z and θ . Therefore, the Hamiltonian of the projected system is written as $H = \lambda_1 \cos \psi + \lambda_2 \sin \psi + \lambda_5 u_h + 1$. This, corresponds to the Hamiltonian equation of a *Dubins* car, with only the heading angular velocity u_h as a control. \square

Table II. List of five-piece 3D paths generated using the geometric method with their corresponding PMP extremals.

Five-piece 3D Path	PMP type
H_2, H_1, S, H_1, H_2	Type 4 Type 2 Type 1 Type 2 Type 4
H_2, C, S, H_1, H_2	Type 4 Type 3 Type 1 Type 2 Type 4
H_2, H_1, S, C, H_2	Type 4 Type 2 Type 1 Type 3 Type 4
H_2, C, S, C, H_2	Type 4 Type 3 Type 1 Type 3 Type 4
H_2, S, H_2	Type 4 Type 1 Type 4

Type 3: ($\lambda_4 \neq 0$ and $\lambda_5 = 0$) The path is a vertical Dubins path existing in a plane normal to (x, y) -plane of equation $c_1y - c_2x + c_5 = 0$.

Proof. $\lambda_4 \neq 0$ then, by using Eq. (14), $u_p = \text{sign}(\lambda_4)$. Since, $\lambda_5 = 0$ then the condition $c_1y - c_2x + c_5 = 0$ still holds, that is, the heading angle ψ is constant. Accordingly, in this case the Hamiltonian of the system is independent of λ_5 and would be represented as $H = (\lambda_1 \cos \psi + \lambda_2 \sin \psi) \cos \theta + \lambda_3 \sin \theta + \lambda_4 u_p + 1$. This Hamiltonian corresponds to a vertical Dubins car with only the pitch angular velocity as control, along with the condition $c_1y - c_2x + c_5 = 0$. □

Type 4: ($\lambda_4 \neq 0$ and $\lambda_5 \neq 0$) In this case, it is clear from Eqs. (14) and (15) that $u_p = \text{sign}(\lambda_4)$ and $u_h = \text{sign}(\lambda_5)$.

Proof. In this case, both controls are saturated, that is, acquiring their maximum allowable values ($u_p = \pm 1$ and $u_h = \pm 1$). Thus, from the kinematic model, $\dot{\theta}(t) = u_p = \pm 1$ and $\dot{\psi}(t) = u_h = \pm 1$. Accordingly, one can integrate to solve for the pitch and yaw angles to get $\theta(t) = \pm t + k_4$ and $\psi(t) = \pm t + k_5$, where k_4 and k_5 are constants of integration. Finally, the non-planar trajectory traversed by the vehicle can be parameterized by arc-length to get

$$\begin{aligned} \dot{x}(t) &= \cos(\pm t + k_5) \cos(\pm t + k_4), \\ \dot{y}(t) &= \sin(\pm t + k_5) \cos(\pm t + k_4), \\ \dot{z}(t) &= \sin(\pm t + k_4). \end{aligned} \tag{16}$$

It is evident that the curve types obtained using our proposed geometric method all correspond to one of the four types of candidates obtained using the PMP. Curve H_1 is correspondent to *Type 2* of the optimal paths, whereas curve H_2 is correspondent to *Type 4* of the optimal paths. Table II links every possible configuration of the 3D path to its correspondent type in the PMP family of minimizer curves. These results clearly show that the paths generated by the proposed geometric method satisfy, piecewisely, the conditions for optimality imposed by the PMP. □

5. 3D Paths Extension

In this section, the robustness of the proposed geometric method is investigated by examining its applicability to extreme configurations.

5.1. 3D paths with CCC-type horizontal Dubins path

In the previous examples, all 3D paths were constructed by using the CSC type of the Dubins paths. Normally, a CCC configuration is feasible when the vertical projections of the initial and final positions are relatively close to each other, specifically when the Euclidian distance between the two positions is less than the minimum allowed diameter of curvature ($< 2R$). In this case, the CCC Dubins configuration is used as a horizontal path in the 3D reconstruction. As for the vertical path, although a CCC path is geometrically possible, such a path is practically infeasible for a real vehicle described by the kinematic model in Eq. (1).

Such a CCC path in the vertical sub-problem will require the vehicle to perform a flip maneuver. This is due to the fact that for optimal CCC-type paths, the arc length of the middle circle must be

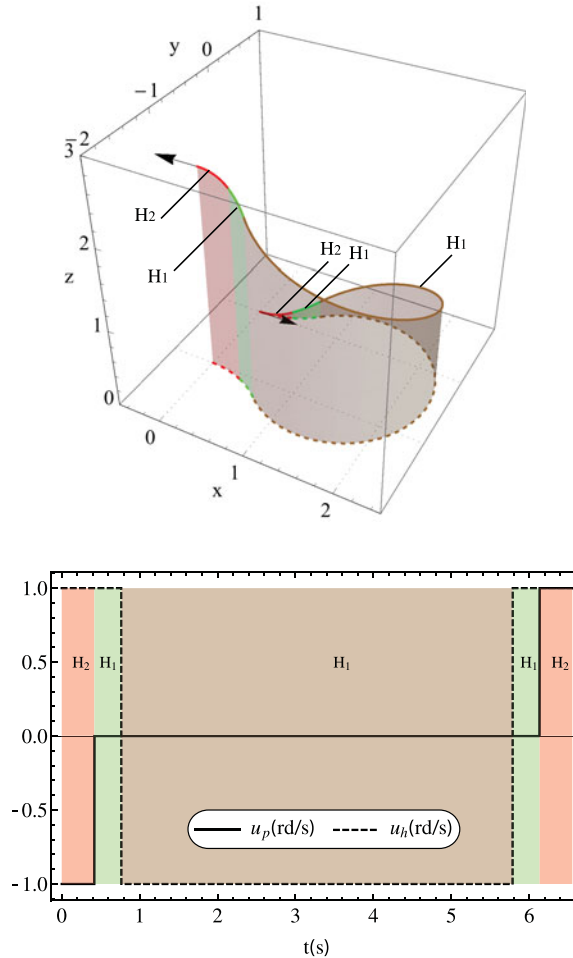


Fig. 7. 3D path with CCC-type horizontal Dubins path with the control input.

greater than π radians as was proved in ref. [5] This would violate the maximum climbing angle constraint.

Accordingly, in the case where the horizontal sub-problem yields a CCC path, the 3D solution type curves are similar to those of the 3D curves presented earlier, except for the straight line sub-path that is replaced by an H_1 -type curve. A complete 3D path is shown in Fig. 7.

5.2. Motion constraints and high-altitude configurations

One of the major restricting constraints for 3D maneuvering vehicles is the vertical maximum climbing angle α_{max} , which is limited due to the action of the control actuators. In general, the climbing angle describes the rate of change of altitude (z), which should not be confused with the pitch angle θ . However, for the scope of this paper, the heading vector of the vehicle is assumed to be tangent to the path at all times, and thus the climbing and pitch angles coincide, i.e., ($\alpha = \theta$).

The boundedness of the pitch angle results in two distinct cases in the path planning method. A low-altitude configuration, where the altitude of the goal position lies beneath the value allowed by the maximum pitch angle constraint, i.e., neglecting the arc portions of the curve, then $\tan \theta_{max} < \frac{z_f}{x_f}$, and a high-altitude configuration where the vehicle cannot reach its goal destination using the method described above.

In order to overcome the constraint discussed above, we augment the generated 3D path with a well-defined helical path. In more details, when tracing the vertical path Γ_v , the length of the unfolded Dubins surface is extended by segments of length 2π so that the value of the pitch angle along the curve Γ_v becomes less than or equal to the maximum allowed value.

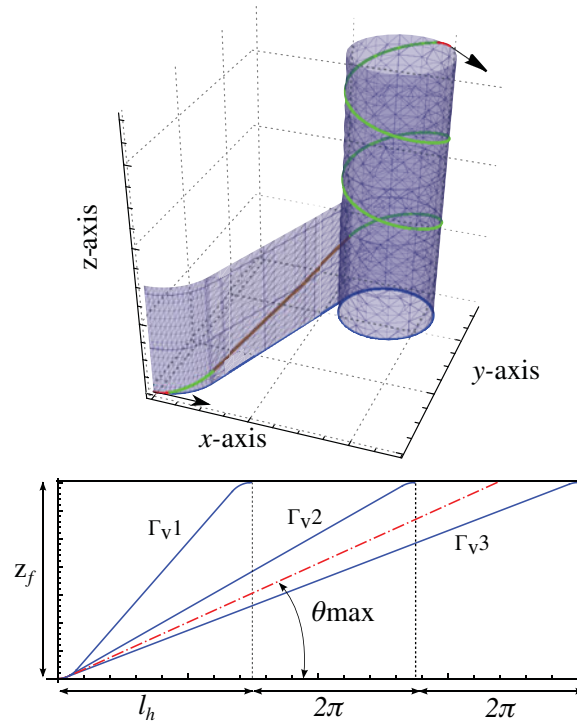


Fig. 8. High-altitude 3D path.

This extension of the Dubins surface is represented by adding circles over any one of the arcs of the horizontal Dubins path Γ_h . Referring to Fig. 8, the length of the Dubins surface was extended twice by adding 2π to the second arc, so that the vertical Dubins path Γ_v3 satisfies the maximum pitch boundary. In other words, the tangent angle to the vertical Dubins path, never exceeds the maximum climb angle. Note that, the additional length could have been added to the first arc with no effect on the total length of the 3D path.

Another extreme case is one where the desired altitude is right above the initial configuration, i.e., $q_f = (0, 0, z, 0, \theta_f)$. In this case, the final configuration is problematic at both the horizontal and vertical levels. However, using a single C segment to solve the horizontal sub-problem, as was mentioned in Section 3.1, and then combining this with the idea of augmenting a helical path in the vertical direction, the final configuration can now be reached while respecting all constraints, and the proposed geometric method remains applicable, proving its robustness. Figure 9 depicts an example where the solution curve is found for $q_i = (0, 0, 0, 0, 0)$ and $q_f = (0, 0, 5, 0, 0)$. The case where the desired altitude is very high and the desired horizontal movement is very small is depicted in Fig. 10. In this case, the solution to the horizontal sub-problem is CSC, where the small S portion is the orange vertical band on the figure. Three additional turns were required in the vertical direction to ensure that the maximum climb angle constraint is not violated.

5.3. Motion for underwater vehicles in gliding mode

Most autonomous underwater vehicles operate in two modes: thrust mode and gliding mode. When in gliding mode, i.e., when the thrusters are turned off, the vehicle can only navigate with low velocity. This results in a large minimum turning radius in the vertical direction. As a result, the limits on the heading and pitch rates become different. Moreover, the gliding mode also limits the attainable climb angles; the maximum allowable climb angle becomes smaller in the gliding mode.

Our proposed geometric method is robust enough to deal with such conditions. First of all, due to the “shallow” climb angle constraint, multiple turns need to be added in the vertical direction, to ensure that this constraint is respected at all times. Moreover, a larger minimum allowable turning radius in the vertical direction simply means that the pitch rate control bounds become smaller. In theory, this does not affect the validity or the applicability of the proposed method in any way. An

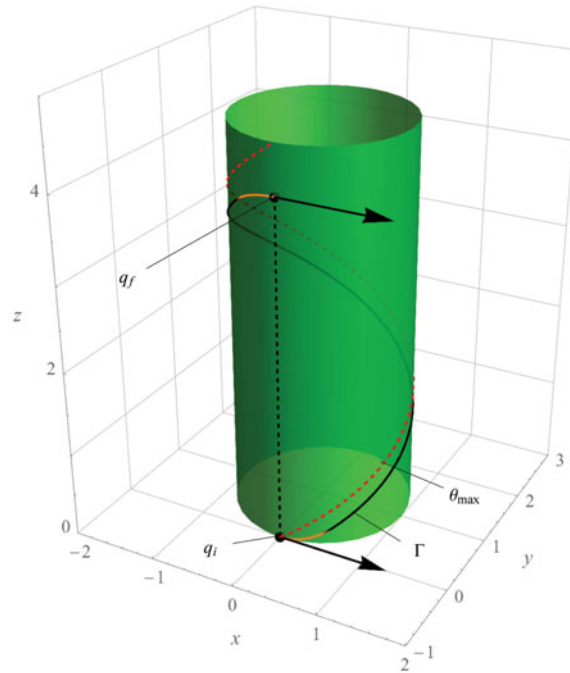


Fig. 9. A high altitude desired configuration, where the solution to the horizontal sub-problem is C.

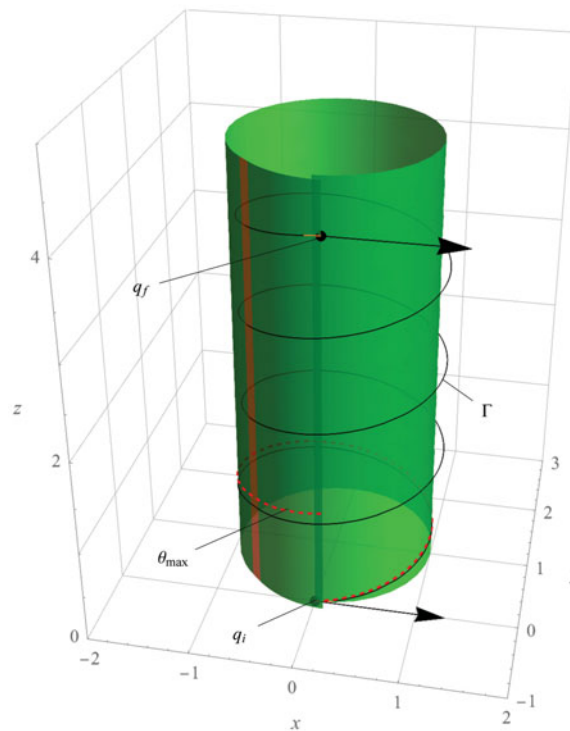


Fig. 10. A high altitude desired configuration, where $q_i = (0, 0, 0, 0, 0)$ and $q_f = (0.1, -0.1, 5, 0, 0)$.

example is showcased in Fig. 11, where $q_f = (5, 5, 4, \frac{-\pi}{2}, 0)$, the maximum allowable climb angle is 10 degrees, and the minimum turning radii in the horizontal and vertical direction, r_h and r_v , are 1 m and 25 m, respectively, which are different by orders of magnitude. This illustrates the robustness of the proposed method to these extreme situations.

Table III. Simulation results for cases 1, 2, and 3.

Case	$(x_f, y_f, z_f, \theta_f, \psi_f)$	Our method			Hota and Ghose			Chitsaz and Lavalle		
		Shortest	Feasible	Applicable	Shortest	Feasible	Applicable	Shortest	Feasible	Applicable
Case 1	$(4, 1, 3, 0^\circ, -45^\circ)$	5.36 m			5.46 m			5.28 m		
		X	✓	✓	X	✓	✓	✓	X	✓
Case 2	$(-4, 0, 3, 0^\circ, 0^\circ)$	10.72 m			10.29 m			10.71 m		
		X	✓	✓	✓	X	✓	X	X	✓
Case 3	$(-4, 5, 3, 30^\circ, 210^\circ)$	9 m			9.11 m			-		
		✓	✓	✓	X	✓	✓	X	X	X

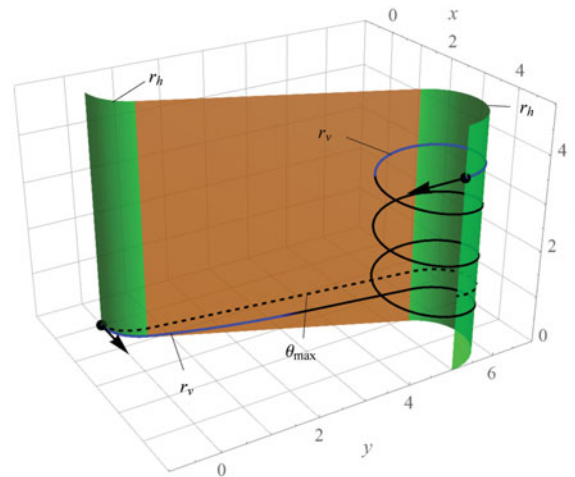


Fig. 11. 3D path for different control bounds in the heading and pitch directions.

6. Simulation Results

This section compares the generated 3D paths to those of Chitsaz and LaValle⁴ and Hota and Ghose,⁹ on the basis of optimality. We chose to compare to these two methods because of their originality and due to the fact that these methods, similar to ours, are based on a geometric approach. Note that, the model used by Chitsaz and LaValle⁴ describes the motion of a 3D maneuvering vehicle by using a four-state kinematic model which neglects any pitch rotation but considers a control over the altitude velocity \dot{z} . However, Hota and Ghose⁹ used a five-state model to describe their method. The numerical method in ref. [9] is not considered in this study, only their geometric approach.

In Table III, three final configurations are given, and the lengths of the resulting paths for the different methods are computed and compared, along with the optimality, feasibility, and applicability of each model. By feasibility we mean whether the vehicle is tangent to the path or the maximum climb angle constraint is satisfied. Applicability indicates whether or not the method can generate a path for the given configuration, that is, the boundary conditions are met.

It is important to mention that these sets of final configurations were specifically chosen to assess the method proposed in this paper with respect to the most relevant methods in literature as it pertains to optimality, robustness, and feasibility. To be precise, the final configurations were chosen to show that while the prior methods produced shorter paths, yet such paths were infeasible. To address the robustness of the method proposed in this paper, for some chosen test configurations, the prior methods even fail to produce a path between the initial and final configurations. In fact, our proposed

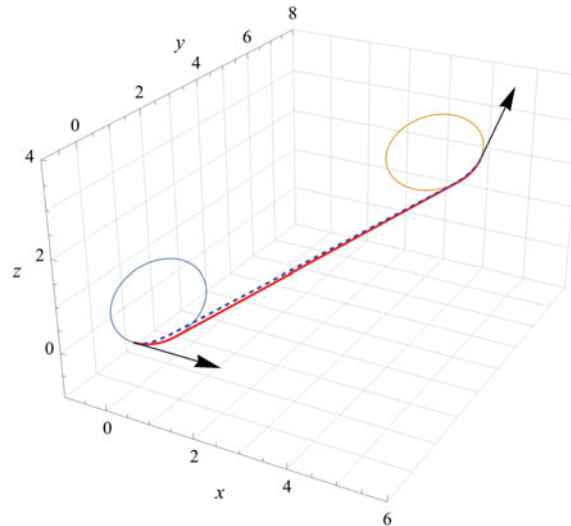


Fig. 12. Our path (dashed blue) vs. Hota and Ghose's path (solid red) for the last entry in Table IV.

method is robust in the sense that it always generates a path which is guaranteed to meet feasibility constraints as shown in Table III. Figure 14 shows the traced paths for the three cases, respectively.

Case 1 $(x_f, y_f, z_f, \theta_f, \psi_f) = (4, 1, 3, 0^\circ, -45^\circ)$: It is obvious that the total length of Chitsaz and LaValle's path is the shortest. Nonetheless, the vehicle's x -axis is not tangent to the path but always parallel to the $x - y$ plane, i.e., it is assumed that the vehicle can ascend/descend vertically without the need to change its pitch angle. This is infeasible in practice. Moreover, maintaining a zero pitch angle would subject the vehicle to higher drag forces. Our method produces a relatively longer, yet feasible path. Note also that our generated path is shorter than that of Hota and Ghose's.

Case 2 $(x_f, y_f, z_f, \theta_f, \psi_f) = (-4, 0, 3, 0^\circ, 0^\circ)$: Hota and Ghose's path is the shortest but not feasible for a real vehicle with constraint on its maximum pitch angle. This is clear since the vehicle has to perform a "flip" ($\theta > 180^\circ$), as shown in case 2 in Fig. 14. In this case, our method produces the longest but still the "only feasible" path among the two other methods.

Case 3 $(x_f, y_f, z_f, \theta_f, \psi_f) = (-4, 5, 3, 30^\circ, 210^\circ)$: In the case, where the final pitch angle is not zero, the method of Chitsaz and LaValle is not applicable since it neglects any pitch angle rotation. Moreover, our method gives a shorter path than that of Hota and Ghose.

Since Hota and Ghose's method is the only method capable of producing feasible paths, we present more simulations in Table IV for a more involved comparison. For the final configuration, we used $(x_f, y_f, z_f, \theta_f, \psi_f) = (5, 5, 3, \theta_f, 90^\circ)$, and the pitch angle was varied between -30° and $+30^\circ$. The results in the table clearly show that our method produces a slightly shorter, and hence more optimal path, for each case presented. Figure 12 illustrates the paths obtained for the last entry in Table IV.

7. Discussion

It is noteworthy to mention that while our proposed approach guarantees local optimality, it does not guarantee global optimality. This in fact roots back to Pontryagin's Principle itself and the fact that it only gives the necessary conditions for an optimal path but not the sufficient ones. Global optimality is investigated in the *path synthesis* problem: given two configurations, what is the optimal concatenation of the candidate locally, optimal segments. This is out of the scope of this paper, and we leave it for future work.

Moreover, we find it important to stress the fact that the proposed decomposition of the problem into two sub-problems, a horizontal and vertical one, and solving them in the order specified, i.e., the horizontal at first, is the optimal, and in fact the only manner with which the decomposition

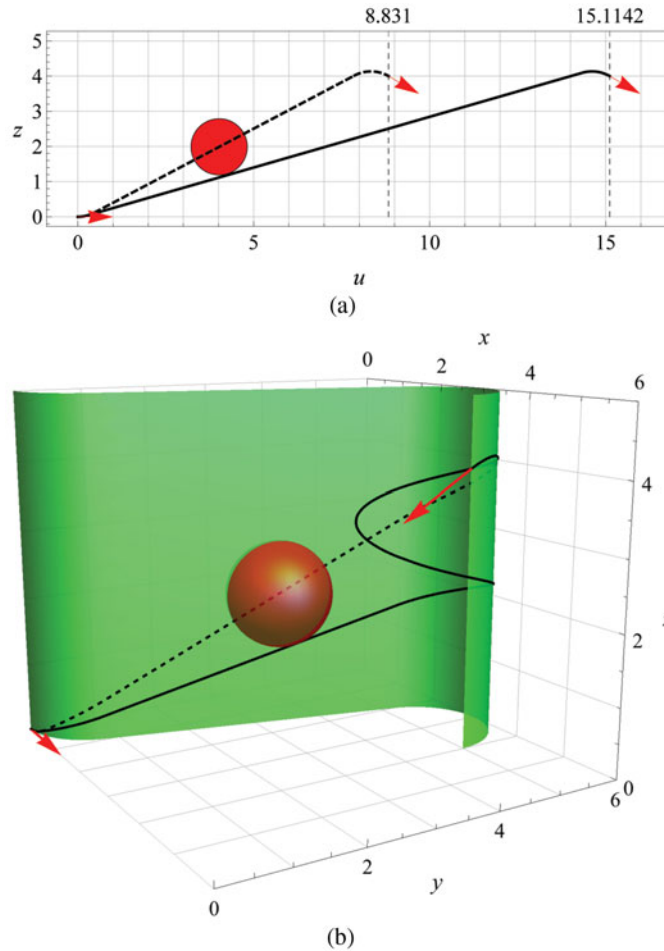


Fig. 13. Modifying the climb angle constraint to avoid obstacles.

can be performed. In other words, projecting the problem onto the horizontal plane at first is the only possible projection that maintains optimality of the paths and ensures that the climbing angle constraint is respected. In fact, since the climbing angle constraint is specified in the vertical direction, then the initial projection of the problem must be onto the horizontal plane. In the general case, the initial projection must always be performed onto a plane perpendicular to the one containing the configuration constraints.

An interesting extension to the problem, which the authors would like to pursue in future work, is the case where obstacles are present in the environment. The aim is to adapt the proposed method such that it tackles the optimal, obstacle-avoiding problem. Our hypothesis is that the obstacles can be represented as constraints on the configuration space, similar to the climbing angle constraint. As such, our proposed approach would remain applicable, and the decomposition would need to be performed in a manner that respects the new constraints. For example, consider the dashed vertical Dubins path in Fig. 13(a), which is impeded by the presence of the obstacle. To overcome this, the vertical sub-problem needs to be solved with the maximum angle constraint modified such that the vehicle maneuvers under the obstacle. Note that since the vehicle cannot maneuver at an angle greater than the maximum climb angle, then it can only pass under the obstacle in the vertical direction, and not above it. The solid line in Fig. 13(a) represents the solution to the vertical Dubins problem with the maximum climb angle modified such that the vehicle barely avoids the obstacle. The horizontal solution path was lengthened by a single turn to achieve a lower maximum climbing angle that clears the obstacle. Figure 13(b) depicts the resulting, obstacle-avoiding path in 3D.

It is noteworthy to mention that we have only introduced a preliminary idea of how the problem of obstacle avoidance may fit into our proposed framework. We have only dealt with static obstacles

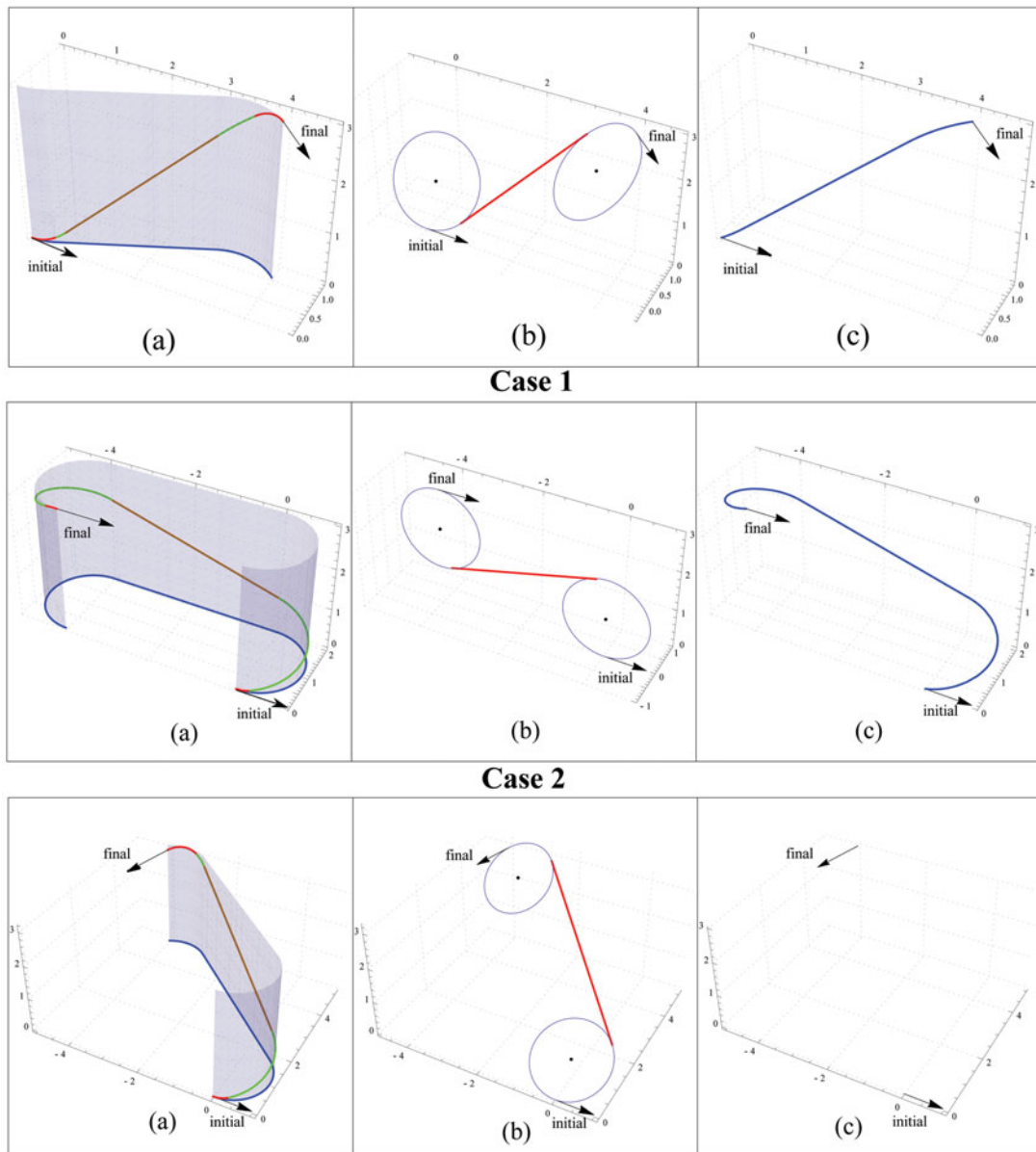


Fig. 14. Comparing 3D path planning methods: (a) Our method, (b) Hota and Ghose, and (c) Chitsaz and LaValle.

with simple geometries. On the other hand, dynamic obstacles or ones with a complicated shape would certainly require a more delicate treatment, which is left for future work.

8. Conclusion

In this paper, we presented a kinematic model of a vehicle that maneuvers in 3D space respecting the boundedness of the heading and pitch curvatures. In Section 3, a geometric method was devised to generate feasible 3D trajectories between two given positions and orientations, by using the results of optimal 2D trajectories. By feasible we mean, respecting pitch and heading rotational velocity constraints as well as the maximum climb and descent angles. Then in Section 4, we used PMP as a necessary condition to find out a family of minimizer curves which could be traced by the 3D kinematic model in Eq. (1). Accordingly, we showed that the paths generated by our proposed method are composed of concatenations of at most five pieces, each of which is a member of the family of minimizer curves characterized by the PMP. Moreover, the proposed geometric method was extended

Table IV. Optimality length comparison for $(x_f, y_f, z_f, \theta_f, \psi_f) = (5, 5, 3, \theta_f, 90^\circ)$.

Pitch angle, θ_f	Hota and Ghose	Our path
-30°	8.0758 m	7.9754 m
-15°	7.9619 m	7.8874 m
0°	7.8915 m	7.8473 m
$+15^\circ$	7.8547 m	7.8365 m
$+30^\circ$	7.8428 m	7.8363 m

to include paths with CCC-type horizontal Dubins projections and high-altitude configurations, thus allowing to reach any desired final position and orientation within the configuration space, without violating the constraints. This highlights the method's capability of dealing with complex motion constraints.

References

1. R. Alterovitz *et al.*, "Motion planning under uncertainty for image-guided medical needle steering," *Int. J. Robot. Res.* **27**(11–12), 1361–1374 (2008).
2. A. Balluchi *et al.*, "Path Tracking Control for Dubin's Cars," *Proceedings of IEEE International Conference on Robotics and Automation (ICRA)*, Minneapolis, MN, USA, vol. 4 (1996) pp. 3123–3128.
3. J.-D. Boissonnat *et al.*, "Shortest Paths of Bounded Curvature in the Plane," *Proceedings of 1992 IEEE International Conference on Robotics and Automation*, Nice, France, vol. 3 (1992) pp. 2315–2320.
4. H. Chitsaz and S. M. LaValle, "Time-Optimal Paths for a Dubins Airplane," *Proceedings of the 46th IEEE Conference on Decision and Control*, New Orleans, Louisiana, USA (2007) pp. 2379–2384.
5. L. E. Dubins, "On curves of minimal length with a constraint on average curvature, and with prescribed initial and terminal positions and tangents," *Am. J. Math.* **79**(3), 497–516 (1957).
6. V. Duindam *et al.*, "Three-dimensional motion planning algorithms for steerable needles using inverse kinematics," *Int. J. Robot. Res.* **29**(7), 789–800 (2010).
7. A. A. Furtuna and D. J. Balkcom, "Generalizing Dubins curves: Minimum-time sequences of body-fixed rotations and translations in the plane," *Int. J. Robot. Res.* **29**(6), 703–726 (2010).
8. O. Gal and Y. Doytsher, "Fast and efficient visible trajectories planning for the Dubins UAV model in 3D built-up environments," *Robotica* **32**(01), 143–163 (2014).
9. S. Hota and D. Ghose, "Optimal Path Planning for An Aerial Vehicle in 3D Space," *Proceedings of the 49th IEEE Conference on Decision and Control*, Atlanta, Georgia, USA (2010) pp. 4902–4907.
10. K. Jiang *et al.*, "Time-optimal smooth-path motion planning for a mobile robot with kinematic constraints," *Robotica* **15**(05), 547–553 (1997).
11. S. Karaman and E. Frazzoli, "Sampling-based algorithms for optimal motion planning," *Int. J. Robot. Res.* **30**(7), 846–894 (2011).
12. Y. Li *et al.*, "Sparse Methods for Efficient Asymptotically Optimal Kinodynamic Planning," *In: Algorithmic Foundations of Robotics XI* (H. Levent Akin, Nancy M. Amato, Volkan Isler and A. Frank van der Stappen, eds.) (Springer 2015) pp. 263–282.
13. N. Mahmoudian *et al.*, "Dynamics and control of underwater gliders I: Steady motions," Tech. rep., Technical Report, Virginia Polytechnic Institute and State University (2009).
14. A. A. Markov, "Some examples of the solution of a special kind of problem on greatest and least quantities," *Soobshch. Karkovsk. Mat. Obshch* **1**, 250–276 (1887).
15. T. G. McGee and J. K. Hedrick, "Optimal path planning with a kinematic airplane model," *J. Guid. Control Dyn.* **30**(2), 629–633 (2007).
16. A. A. Neto and M. F. M. Campos, "A Path Planning Algorithm for UAVs with Limited Climb Angle," *Proceedings of IEEE/RSJ International Conference on Intelligent Robots and Systems (IROS)*, Saint Louis, Missouri, USA (2009) pp. 3894–3899.
17. G. Papadopoulos, Asymptotically Optimal Path Planning and Surface Reconstruction for Inspection *Ph.D. Thesis*, Cambridge, Massachusetts, USA (Massachusetts Institute of Technology, 2014).
18. G. Papadopoulos *et al.*, "Analysis of asymptotically optimal sampling-based motion planning algorithms for Lipschitz continuous dynamical systems," (2014) *arXiv preprint arXiv:1405.2872*.
19. L. Pontryagin *et al.*, *The Mathematical Theory of Optimal Processes* (John Wiley, Interscience, New York, 1962).
20. J. Reeds and L. Shepp, "Optimal paths for a car that goes both forwards and backwards," *Pac. J. Math.* **145**(2), 367–393 (1990).
21. H. J. Sussmann, "Shortest 3-Dimensional Paths with a Prescribed Curvature Bound," *Proceedings of the 34th IEEE Conference on Decision and Control*, New Orleans, Louisiana, USA, vol. 4 (1995) pp. 3306–3312.
22. H. J. Sussmann and G. Tang, "Shortest paths for the Reeds-Shepp car: A worked out example of the use of geometric techniques in nonlinear optimal control," *Rutgers Cent. Syst. Control Tech. Rep.* **10**, 1–71 (1991).

23. R. J. Webster *et al.*, “Nonholonomic modeling of needle steering,” *Int. J. Robot. Res.* **25**(5–6), 509–525 (2006).
24. B. Wehbe *et al.*, “A Novel Method to Generate Three-Dimensional Paths for Vehicles with Bounded Pitch and Yaw,” *Proceedings of IEEE International Conference on Advanced Intelligent Mechatronics (AIM)*, Busan, South Korea (2015) pp. 1701–1706.
25. B. Wehbe *et al.*, “Dynamic Modeling and Path Planning of a Hybrid Autonomous Underwater Vehicle,” *Proceedings of the IEEE International Conference on Robotics and Biomimetics (ROBIO)*, Bali, Indonesia (2014) pp. 729–734.
26. E. K. Xidias and N. A. Aspragathos, “Motion planning for multiple non-holonomic robots: A geometric approach,” *Robotica* **26**(04), 525–536 (2008).